Journal of Biomechanics 95 (2019) 109323

Contents lists available at ScienceDirect

Journal of Biomechanics

journal homepage: www.elsevier.com/locate/jbiomech
www.JBiomech.com

Short communication

On the computation of hemodynamic forces in the heart chambers

Gianni Pedrizzetti *

Department of Engineering and Architecture, University of Trieste, Italy

ARTICLE INFO

Article history:
Accepted 23 August 2019

Keywords:
Cardiac fluid dynamics
Hemodynamic forces
Intraventricular pressure gradient
Cardiovascular imaging

ABSTRACT

The hemodynamic forces exchanged between the blood flowing in the heart and the myocardium are recently receiving attention as an important marker of cardiac function. The increasing interest was associated to the advent of advanced imaging methods able to measure the blood velocity field inside the cardiac chambers, from which flow forces are obtained as volume integral of the fluid momentum. These technologies, however, require costly equipment and time-consuming procedures. A different formulation of the balance of momentum, introduced here, permits the computation of hemodynamic forces from geometric and velocity data at the boundary of the blood volume, without the need of measuring the blood velocity inside. This method is valid in generic geometry and is verified in a relatively complex geometry by comparison with results from direct numerical simulation. This approach may permit to integrate the description of cardiac function based on volumetric changes and myocardial deformation with those of hemodynamic forces.

© 2019 Elsevier Ltd. All rights reserved.

1. Introduction

A fluid moving inside a solid deformable container, and possibly moving in and out of it, exchanges forces that impact on the resistance and long-term deformation of the container. In general, the understanding of the reciprocal stresses between a flowing fluid and the surrounding structural boundary represents a fundamental topic in many branches of physics and engineering, from hydraulic systems to civil and industrial implants. In cardiology, the dynamics of blood flowing across the cardiac chambers is known to participate intimately to the cardiac function (Kilner et al., 2000; Pedrizzetti et al., 2014). Here, the hemodynamic forces exchanged between blood and the surrounding tissue were demonstrated to influence the morphogenesis of embryonic hearts (Culver and Dickinson, 2010; Hove et al., 2003) and, more recently, they were recognized to have a role in modulating the response to pathologies in adult hearts (Arvidsson et al., 2018; Eriksson et al., 2017; Lapinskas et al., 2018; Pedrizzetti et al., 2016; Sjöberg et al., 2018).

Recent advances in medical imaging technology (echocardiography and cardiac magnetic resonance) permit, to some extent, to evaluate the blood velocity *in vivo* in regions of physiological interest, like the cardiac chambers or the aortic artery. Once the velocity field is known, the rate of change of momentum the fluid inside a volume $V(t)$ must be balanced with the total hemodynamic forces acting on that volume. Calling $\boldsymbol{F}(t)$ the global hemodynamic force vector the balance of momentum reads

$$\boldsymbol{F}(t) = \int_{V(t)} \rho \frac{\partial \boldsymbol{v}}{\partial t} dV + \int_{S(t)} \rho \boldsymbol{v}(\boldsymbol{v} \cdot \boldsymbol{n}) dS \tag{1}$$

where $\boldsymbol{v}(\boldsymbol{x}, t)$ is the fluid velocity vector field measured at fixed points $\boldsymbol{x}$ at time t, $S(t)$ is the closed surface bounding the volume and $\boldsymbol{n}$ is the outward unit normal vector. The force $\boldsymbol{F}(t)$ is composed of the pressure gradient integrated on the volume (which is equivalent to the pressure integrated with the normal on the surface) plus the viscous forces that are commonly negligible.

The surface integral in (1) can be transformed in a volume integral by the Gauss theorem and, in the case of incompressible fluid, can be rewritten as

$$\boldsymbol{F}(t) = \rho \int_{V(t)} (\frac{\partial \boldsymbol{v}}{\partial t} + \boldsymbol{v} \cdot \nabla \boldsymbol{v}) dV \tag{2}$$

Based on Eq. (2), hemodynamic forces evaluated from medical imaging were introduced as a mathematically well-defined global measure of cardiac function. This approach was used in echocardiography (Pedrizzetti et al., 2015) and, more recently, in three-dimensional/three-directional phase-contrast magnetic resonance imaging (MRI), commonly referred as 4D flow MRI in both the left (LV) and the right (RV) ventricles of the human heart (Arvidsson et al., 2017; Eriksson et al., 2016; Töger et al., 2018). Based on these

* Address: Department of Engineering and Architecture, University of Trieste, P.le Europa 1, 34127 Trieste, Italy.
E-mail address: giannip@dia.units.it

https://doi.org/10.1016/j.jbiomech.2019.109323
0021-9290/© 2019 Elsevier Ltd. All rights reserved.

technologies, the assessment of hemodynamic forces is gaining increasingly interest as an important marker of cardiovascular function.

However, these approaches present important technical difficulties. Fluid velocity evaluated by ultrasound is not accurate. The usage of 4D Flow MRI is more reliable; nevertheless, it requires costly equipment in fixed installation, and time-consuming procedures for both acquisition and post-processing that may not be recommended for estimating a single parameter. They also involve a technical challenge, in the application of formula (1) or (2) to unsteady flow with deformable boundaries, when integrating the time derivatives of velocities at fixed positions in a volume that changes during the cardiac motion.

In order to overcome these difficulties, a simplified methods was introduced to estimate flow-forces inside the LV on the basis of the motion of the surrounding boundary that can be recorded with relative ease in echocardiography or from simple cine cardiac MRI (Pedrizzetti et al., 2017). However, that method is approximate and applies only to the LV when it has a sufficiently regular geometry.

The purpose of this letter is to show that that the hemodynamic flow inside a generic closed volume can be computed from information measured at its boundary only. This method, that is relatively simple and theoretically exact, is verified with results from direct numerical simulation in a relatively complex geometry.

2. Methods I: Mathematical analysis

This sections shows that Eq. (1) can be rewritten in terms of a surface integral. To this aim, consider the generic i-th component of the term inside the volume integral in Eq. (1) that can be rewritten

$$\frac{\partial v_i}{\partial t} = \frac{\partial}{\partial t}\left(\frac{\partial x_i v_k}{\partial x_k}\right) = \frac{\partial}{\partial x_k}\left(x_i \frac{\partial v_k}{\partial t}\right) \tag{3}$$

where summation over repeated index is implicitly assumed. Last passage in (3) assumed that the fluid is incompressible and its divergence is zero. Moreover, the partial time derivative in (3), as well as in (1) and (2), measures time changes at fixed spatial positions, and does not acts on the position vector x_i; in other words, it represents the inertial acceleration and should not include convective acceleration that is already accounted in the last term on the right-hand side of (1) or (2). Last terms in (3) has the form of a divergence and its volume integral can be transformed in a surface integral by the Gauss theorem

$$\int_{V(t)} \frac{\partial v_i}{\partial t} dV = \int_{V(t)} \frac{\partial}{\partial x_k}(x_i \frac{\partial v_k}{\partial t}) dV = \int_{S(t)} x_i \frac{\partial v_k}{\partial t} n_k dS \tag{4}$$

Insertion of the result (4) into Eq. (1) transforms it in an equivalent equation that contains only integrals over the volume surface

$$\boldsymbol{F}(t) = \rho \int_{S(t)} [\boldsymbol{x}(\frac{\partial v}{\partial t} \cdot \boldsymbol{n}) + \boldsymbol{v}(\boldsymbol{v} \cdot \boldsymbol{n})] dS \tag{5}$$

which is valid for incompressible flows.

This approach uses the mass conservation (velocity with zero divergence) and it is important that the velocity field at the boundaries effectively satisfy this constraint.

$$\int_{S(t)} v_n dS = 0 \tag{6}$$

when Eq. (6) is not verified by data (due to noise in recording or other approximations), a correction should be considered to ensure consistency of the boundary velocity with fluid incompressibility.

In the application of Eq. (5), it must be underlined that the fluid velocity on the solid parts of the boundary corresponds to the velocity of the boundary itself for impermeability and adherence. Differently, the velocity of the fluid crossing the open boundaries has to be measured directly. When this is not available, it can be estimated by mass balance (6)

$$\int_{S_{closed}} v_n dS = -\int_{S_{open}} v_n dS \tag{7}$$

Then, when the velocity at the open valve position can be assumed as mostly unidirectional $\boldsymbol{v} = v_n \boldsymbol{n}$ and approximately uniform across the section, an estimation of the velocity vector therein can be provided by

$$\boldsymbol{v} \cong -\frac{\boldsymbol{n}}{S_{open}} \int_{S_{closed}} v_n dS \tag{8}$$

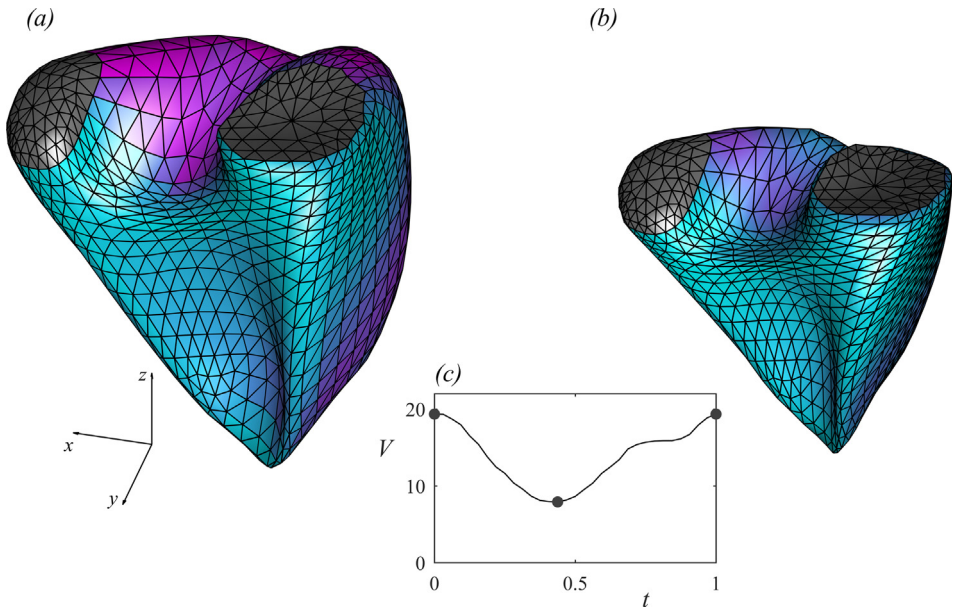

Fig. 1. Geometry of a right ventricle at end-diastole (a) and at end-systole (b). The external surface is described by a triangular mesh, valvular orifices are colored in gray, the coordinate unit vectors (length 1 cm) are reported on (a) for reference. The inset (c) shows the volume curve during one heartbeat, circles indicate the end-diastolic and end-systolic values (units: volume [cm^3], time [s]).

3. Methods II: Numerical verification

The reliability of Eq. (5) is verified by comparison with a numerical simulation of fluid flow performed in the complex cavity shape of a right ventricle (RV). The RV geometry was extracted from three-dimensional echocardiography at 32 instants during one heartbeat and segmented by 938 triangular elements. Fig. 1 shows the RV surface at two instants corresponding to the maximum and minimum volumes as indicated in the inset. The numerical simulation is performed by the immersed boundary method, as previously described (Mangual et al., 2012), using a high resolution $256 \times 192 \times 256$ grid (spacing about 0.03 cm) with an explicit 3rd order Runge-Kutta time advancement and using 4096 time steps per heartbeat to well ensure diffusive and convective stability conditions (taking about 80 h in a workstation). The boundary at all required time instants was obtained by linear interpolation from the 32 available phases. The hemodynamic force is then computed by the numerical velocity solution using Eq. (1); it is also evaluated by Eq. (5) using the given boundary velocity profile in both the open and closed parts, to ensure a punctual comparison. The surface integral in (5) is performed by summation of individual triangular contributions.

4. Results

The result of the comparison are reported in Fig. 2 for the individual components of the hemodynamic force. The forces computed from the surface integral were limited to the 32 instants corresponding to the available phases of the RV surface; those from the numerical simulation, computed with higher time resolution, are reported with continuous line. The two results show an excellent agreement, with minor differences that are imputable to the differences in the numerical integrations (one on the volume, the other on a surface) and to the numerical time derivatives.

5. Discussion

The main contribution of this communication is represented by Eq. (5); it demonstrates that the force associated with a fluid volume can be evaluated from measurements taken at the boundaries of the volume irrespective from the flow phenomena developing inside. This equation is not the result of an original model; it is an exact consequence of the Gauss theorem applied to the balance of momentum. This uncommon reformulation allows the

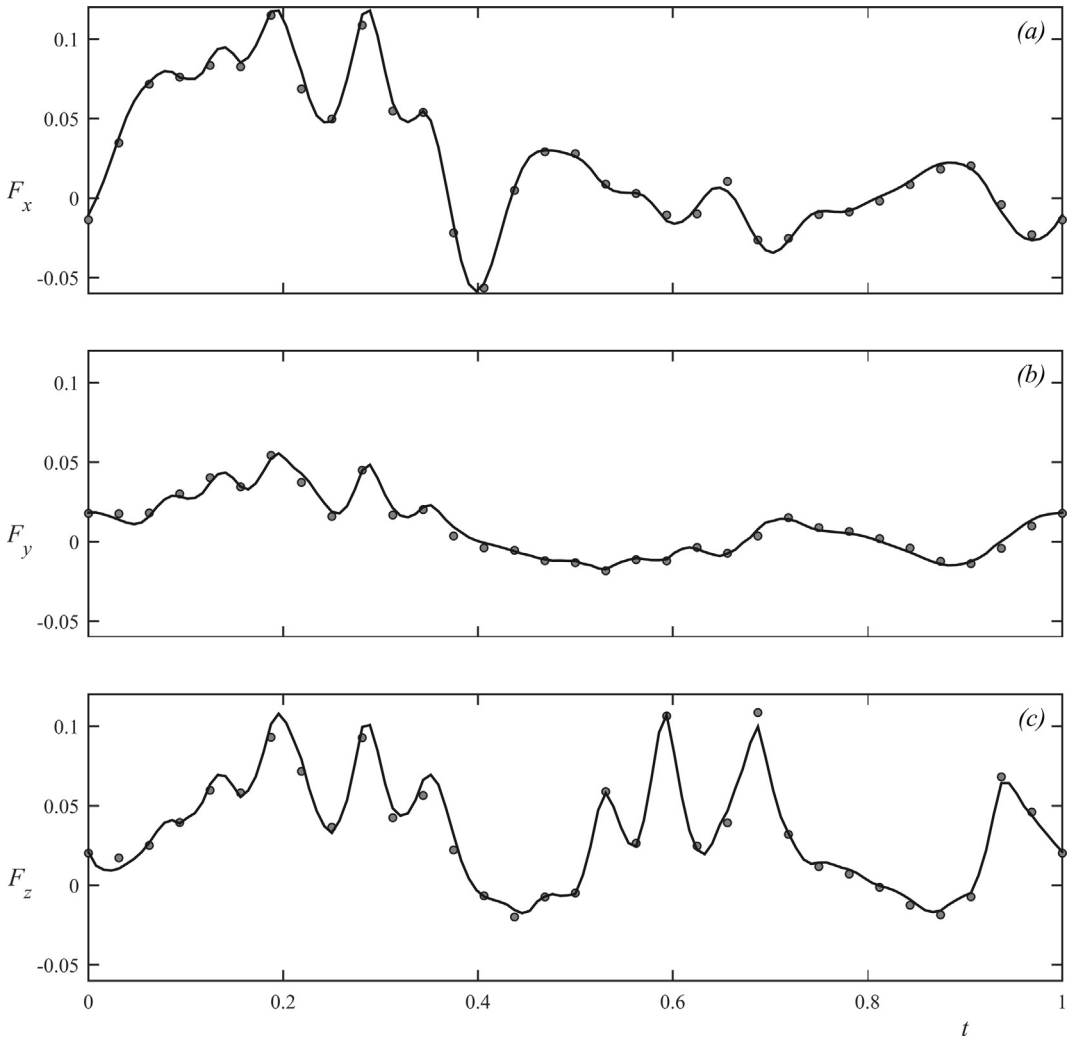

Fig. 2. Comparison between force vector computed from numerical simulation results (continuous line) and from the volume surface (dots). The force vector is reported in dimensionless form, normalized with density, volume and gravity acceleration; time is normalized with the period. The three components are reported, (*a*): $F_x(t)$, (*b*): $F_y(t)$, and (*c*): $F_z(t)$.

estimation of hemodynamic forces without the need of volumetric measurements of fluid velocities.

During last years, cardiovascular imaging technology introduced numerous solutions for estimating the deformation of the LV or RV tissues, they are used to improve the description of cardiac function not only in terms of volumetric changes but also of cardiac strain. (Claus et al., 2015; Muraru et al., 2016; Seo et al., 2014). The formulation introduced here permits to further advance in this direction and includes the assessment of hemodynamic forces based on the same information.

The evaluation of forces exchanged between blood and tissues was always considered a central element of cardiac function that must sustaining blood motion by ensuring the correct propulsion to blood flow (Rushmer, 1964). However, despite their importance, the evaluation of hemodynamic forces (or, equivalently, intraventricular pressure gradients) was limited to animal experiments due to need of invasive catheter procedures (Courtois et al., 1988; Guerra et al., 2013). The applications of hemodynamic forces to clinical cardiology underwent to a rapid acceleration during last years with the advent of imaging technologies able to measure blood velocity *in vivo* (Arvidsson et al., 2018; Eriksson et al., 2017; Pedrizzetti et al., 2016; Sjöberg et al., 2018). The method discussed here can be useful for facilitating their computation when volumetric blood velocities are not available.

The formulation provided by Eq. (5) is theoretically exact; nevertheless, its application presents numerous limitations and potential sources of error. Its reliability depends on the accuracy of the surface information and on their time resolution. It contains tissue velocity and acceleration terms, which usually are not measured directly and are obtained by numerical time derivatives of geometric properties evaluated from medical images, like borders position and velocity, whose accuracy is lower than that of geometric properties themselves. On the other hand, the result is an integral one that can partially smooths out local variabilities. The application of (5) also requires the knowledge of the actual blood velocity in the open parts of the boundary (e.g. for the application in the LV, the mitral flow during diastole and the aortic flow during systole). They can be measured (by cross-plane phase-contrast MRI, or by echo-Doppler, for example) or they can be estimated on the basis of mass balance. In general, evaluations based on formula (5) are influenced by several aspects like imaging modality, spatial accuracy, time resolution, means for measuring valvular flow. A quantification of these uncertainties is not straightforward with theoretical arguments due to the nonlinear relationships present in (5). An extensive sensitivity and comparative analysis in a clinical application context, which is out of the scope of this communication, should be planned to ensure controlled applications.

As a final remark, it is interesting to note that Eq. (5) presents a structure that is formally analogous to the definition of force as the integral of surface stress distribution

$$F(t) = \rho \int_{S(t)} [pn + \tau] dS \tag{9}$$

where p is the pressure field and τ is the viscous stress (usually negligible in a global balance). This analogy, however, does not imply that the specific force term in the integrand of (5) may represent any local surface stress. The equality between Eqs. (9) and (5) is valid only in the integral sense and cannot be extended to the terms inside the integrals.

6. Conclusion

The hemodynamic force exchanged between blood flowing in and out of a cardiac chamber and the surrounding tissue can be computed from a formulation of the balance of momentum that requires geometric and velocity data at the cavity boundary, without the need of measuring the blood velocity inside the chamber's volume. This method is theoretically exact and was verified to be accurate in a model right ventricle. However, its reliability in clinical applications is influenced by several factors and should undergo extensive validations.

Declaration of Competing Interest

The author is consultant and shareholder of AMID SRL (Sulmona, Italy), that has a commercial agreement with TomTec Gmbh (Germany) and Medis BV (The Netherlands) for development of software for deformation imaging in cardiology. This specific work was developed during such a consultancy activity while the author was in temporary leave from his main institution.

References

Arvidsson, P.M., Töger, J., Carlsson, M., Steding-Ehrenborg, K., Pedrizzetti, G., Heiberg, E., Arheden, H., 2017. Left and right ventricular hemodynamic forces in healthy volunteers and elite athletes assessed with 4D flow magnetic resonance imaging. Am. J. Physiol. – Hear. Circ. Physiol. 312, H314–H328. https://doi.org/10.1152/ajpheart.00583.2016.

Arvidsson, P.M., Töger, J., Pedrizzetti, G., Heiberg, E., Borgquist, R., Carlsson, M., Arheden, H., 2018. Hemodynamic forces using 4D flow MRI: an independent biomarker of cardiac function in heart failure with left ventricular dyssynchrony? Am. J. Physiol. Circ. Physiol. ajpheart.00112.2018. https://doi.org/10.1152/ajpheart.00112.2018.

Claus, P., Omar, A.M.S., Pedrizzetti, G., Sengupta, P.P., Nagel, E., 2015. Tissue tracking technology for assessing cardiac mechanics: principles, normal values, and clinical applications. JACC Cardiovasc. Imaging 8, 1444–1460. https://doi.org/10.1016/j.jcmg.2015.11.001.

Courtois, M., Kovács, S.J., Ludbrook, P.A., 1988. Transmitral pressure-flow velocity relation. Importance of regional pressure gradients in the left ventricle during diastole. Circulation 78, 661–671. https://doi.org/10.1161/01.cir.78.3.661.

Culver, J.C., Dickinson, M.E., 2010. The effects of hemodynamic force on embryonic development. Microcirculation 17, 164–178. https://doi.org/10.1111/j.1549-8719.2010.00025.x.

Eriksson, J., Bolger, A.F., Ebbers, T., Carlhäll, C.-J., 2016. Assessment of left ventricular hemodynamic forces in healthy subjects and patients with dilated cardiomyopathy using 4D flow MRI. Physiol. Rep. 4, 741–747. https://doi.org/10.14814/phy2.12685.

Eriksson, J., Zajac, J., Alehagen, U., Bolger, A.F., Ebbers, T., Carlhäll, C.-J., 2017. Left ventricular hemodynamic forces as a marker of mechanical dyssynchrony in heart failure patients with left bundle branch block. Sci. Rep. 7, 2971. https://doi.org/10.1038/s41598-017-03089-x.

Guerra, M., Brás-Silva, C., Amorim, M.J., Moura, C., Bastos, P., Leite-Moreira, A.F., 2013. Intraventricular pressure gradients in heart failure. Physiol. Res. 62, 479–487.

Hove, J.R., Köster, R.W., Forouhar, A.S., Acevedo-Bolton, G., Fraser, S.E., Gharib, M., 2003. Intracardiac fluid forces are an essential epigenetic factor for embryonic cardiogenesis. Nature 421, 172–177. https://doi.org/10.1038/nature01282.

Kilner, P.J., Yang, G.Z., Wilkes, A.J., Mohiaddin, R.H., Firmin, D.N., Yacoub, M.H., 2000. Asymmetric redirection of flow through the heart. Nature 404, 759–761. https://doi.org/10.1038/35008075.

Lapinskas, T., Pedrizzetti, G., Stoiber, L., Düngen, H., Edelmann, F., Pieske, B., Kelle, S., 2018. The intraventricular hemodynamic forces estimated using routine CMR cine images: a new marker of the failing heart. JACC Cardiovasc. Imaging. doi: 10.1016/j.jcmg.2018.08.012.

Mangual, J.O.O., Domenichini, F., Pedrizzetti, G., 2012. Three dimensional numerical assessment of the right ventricular flow using 4D echocardiography boundary data. Eur. J. Mech. B/Fluids 35, 25–30. https://doi.org/10.1016/j.euromechflu.2012.01.022.

Muraru, D., Spadotto, V., Cecchetto, A., Romeo, G., Aruta, P., Ermacora, D., Jenei, C., Cucchini, U., Iliceto, S., Badano, L.P., 2016. New speckle-tracking algorithm for right ventricular volume analysis from three-dimensional echocardiographic data sets: validation with cardiac magnetic resonance and comparison with the previous analysis tool. Eur. Hear. J. – Cardiovasc. Imaging 17, 1279–1289. https://doi.org/10.1093/ehjci/jev309.

Pedrizzetti, G., Arvidsson, P.M., Töger, J., Borgquist, R., Domenichini, F., Arheden, H., Heiberg, E., 2017. On estimating intraventricular hemodynamic forces from endocardial dynamics: a comparative study with 4D flow MRI. J. Biomech. 60, 203–210. https://doi.org/10.1016/j.jbiomech.2017.06.046.

Pedrizzetti, G., La Canna, G., Alfieri, O., Tonti, G., 2014. The vortex – an early predictor of cardiovascular outcome? Nat. Rev. Cardiol. 11. https://doi.org/10.1038/nrcardio.2014.75.

Pedrizzetti, G., Martiniello, A.R., Bianchi, V., D'Onofrio, A., Caso, P., Tonti, G., 2016. Changes in electrical activation modify the orientation of left ventricular flow momentum: novel observations using echocardiographic particle image velocimetry. Eur. Heart J. Cardiovasc. Imaging 17, 203–209. https://doi.org/10.1093/ehjci/jev137.

Pedrizzetti, G., Martiniello, A.R., Bianchi, V., D'Onofrio, A., Caso, P., Tonti, G., D'Onofrio, A., Caso, P., Tonti, G., 2015. Cardiac fluid dynamics anticipates heart adaptation. J. Biomech. 48, 388–391. https://doi.org/10.1016/j.jbiomech.2014.11.049.

Rushmer, R.F., 1964. Initial ventricular impulse. A potential key to cardiac evaluation. Circulation XXIX, 268–283. doi: 10.1161/01.CIR.29.2.268.

Seo, Y., Ishizu, T., Aonuma, K., 2014. Current status of 3-dimensional speckle tracking echocardiography: a review from our experiences. J. Cardiovasc. Ultrasound 22, 49–57. https://doi.org/10.4250/jcu.2014.22.2.49.

Sjöberg, P., Töger, J., Hedström, E., Arvidsson, P.M., Heiberg, E., Arheden, H., Gustafsson, R., Nozohoor, S., Carlsson, M., 2018. Altered biventricular hemodynamic forces in patients with repaired Tetralogy of Fallot and right ventricular volume overload due to pulmonary regurgitation. Am. J. Physiol. Circ. Physiol. ajpheart.00330.2018. https://doi.org/10.1152/ajpheart.00330.2018.

Töger, J., Arvidsson, P.M., Bock, J., Kanski, M., Pedrizzetti, G., Carlsson, M., Arheden, H., Heiberg, E., 2018. Hemodynamic forces in the left and right ventricles of the human heart using 4D flow magnetic resonance imaging: Phantom validation, reproducibility, sensitivity to respiratory gating and free analysis software. PLoS One 13. https://doi.org/10.1371/journal.pone.0195597.